Electrical and Mechanical Characterization of Lateral NEMS Switches

R. Hinchet[1], L. Montès[1], G. Bouteloup[1], G. Ardila[1],
R. Parsa[2], K. Akarvardar[2,3], R. T. Howe[2], H.-S. Philip Wong[2]
[1]IMEP-LAHC, Grenoble Institute of Technology, MINATEC, 3 Parvis Louis Néel, 38016 Grenoble, France
[2]Department of Electrical Engineering, Stanford University, CA 94305, USA
[3]Present affiliation: Globalfoundries/SEMATECH, Albany, NY 12203, USA
Ronan.Hinchet@minatec.inpg.fr Ph : +33 456 529 516

Abstract: **In this paper we present a study on the electrical and mechanical characterization of NEMS Nano Switches. Pull-in, pull-out voltages are in good agreement with the theoretical values. However some reliability and sticking problems are identified. To investigate furthermore the mechanical properties of the nanoswitch (NS) beam, we have developed a dedicated AFM methodology to extract the Young's modulus. A further improvement of the design is then realized based on the results of this study.**

Keywords: **NEMS, Nano-switches, Young's modulus, mechanical characterization, AFM.**

I. INTRODUCTION

Alternative device architectures and solutions might be required to continue the trend described by Moore's Law. NEMS Nano-Switch (NS) [1,2], may open ways for even more complex circuits using fewer components, while lowering the energy consumption due to the complete absence of electrical leakage in the off-state [3]. In this paper we study electrical and mechanical properties of such NS (Fig. 1). The NS concept is based on controlling the current through a mobile beam between electrodes similar to source (S) and drain (D) in a standard MOS device. A gate (G) voltage controls the lateral switch by electrostatically attracting the beam. According to theory, the non-linear behavior of electrostatic forces and Van der Waals forces between the beam and the drain should lead to an hysteresis of the I-V characteristics. The NS was fabricated using one-mask process. It started with a 1.5µm thick LTO and 1.1µm thick doped-poly-silicon deposition, followed by an RTA at 1075°C. The poly-silicon was patterned using deep-UV lithography and a reactive-ion-etch (RIE) [4,5]. The underlying SiO2 sacrificial layer was then removed using a 49% wet HF release to free-stand the beam. Critical Dry Point (CDP) was used to avoid sticking. We checked the beam release and CDP process with Scanning Electron Microscope (SEM) observations (Fig. 2). In most of the cases beams were correctly release. We just noted an over-etching (Fig. 3) on the edge of the connection pads which depends on the length and the concentration of the wet HF release step.

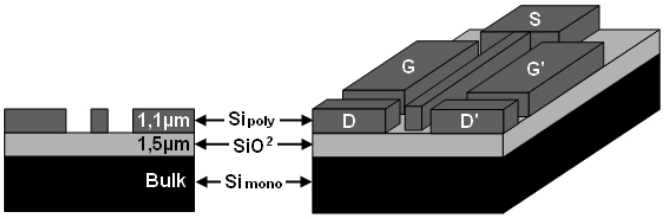

Fig. 1. Structure of a NS. (Source (S), Gate (G), Drain (D)). Beam: 300nm width, 1100 nm thick and 20 µm length.

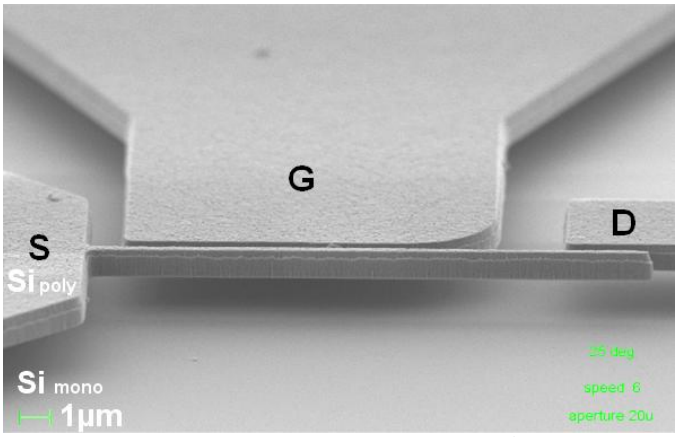

Fig. 2. Scanning Electron Microscopy image of a NS.

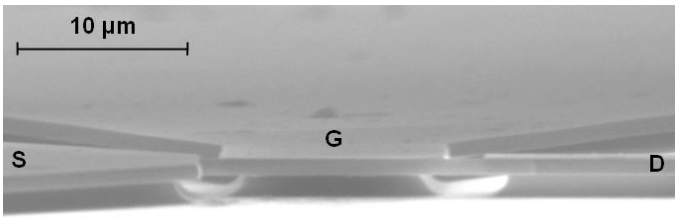

Fig. 3. Scanning Electron Microscopy image of the side of a NS.

II. ELECTRICAL CHARACTERIZATION

Electrical results clearly demonstrated the lateral actuation of the beam (Fig. 4), while showing slightly lower pull-in voltage Vpi and pull-out voltage Vpo (Fig. 5) than expected by theory [1,2]. We noted the importance of the atmospheric environment: care must be taken especially with humidity, working under nitrogen or vacuum ambient lead to an improved yield. We also experienced, on some NS, difficulties to switch on or off (Fig. 6), with part of the NS beam sticking or staying stuck to the drain.

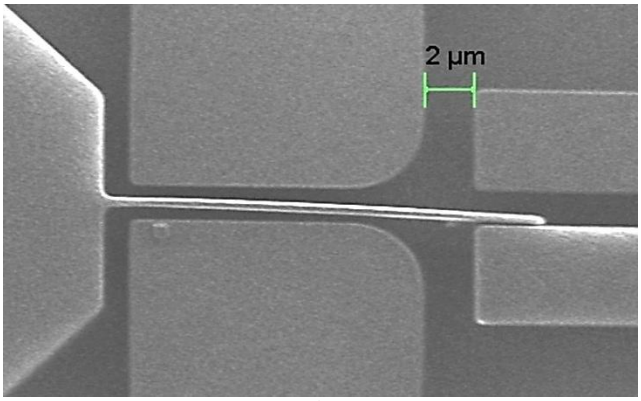

Fig. 4. SEM image of a NS at the ON state.

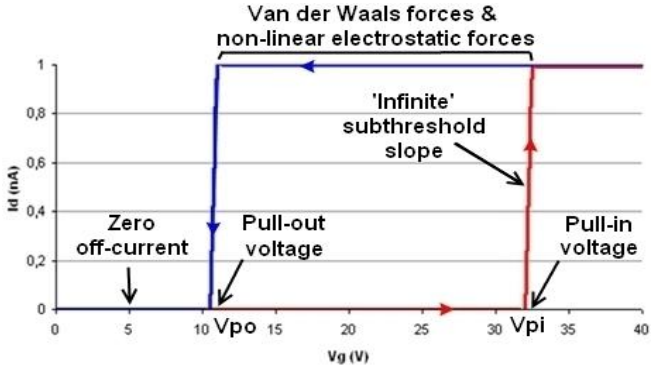

Fig. 5. Experimental electrical characterization of a NS.
Measurement parameters: V_S=0V, V_D=3V, compliance 1nA.

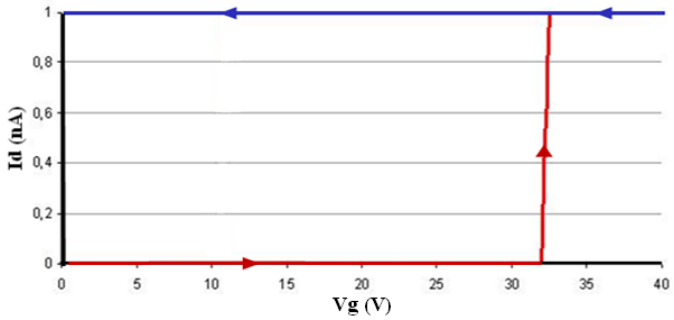

Fig. 6. Experimental electrical characterization of a NS.
The beam staying stuck to the drain after ON state, as shown in Fig. 4.
Measurement parameters: V_S=0V, V_D=3V, compliance 1nA.

III. AFM MECHANICAL CHARACTERIZATION

Mechanical properties of the polysilicon beam were investigated by vertical and local approach-retract curves obtained with an AFM. From the Euler-Bernoulli equation (eq. 1) we calculated the relation between the force applied by the AFM tip and the beam deflection Δz (Fig. 7) [6], where *x* is beam axis, *u* is the position along x where the force is applied, E is the Young's modulus, F is the applied force, Iy is the beam moment (considering a rectangle cross section), l is the beam length, w is the beam width and t is the beam thickness. To calculate the solution to the equation 1 we considered the particular case where we applied the force at the end of the beam.

$$(eq.1) \quad \frac{d^2}{dx^2}\left(E.I_y.\frac{d^2u}{dx^2}\right) = F \quad \rightarrow \quad \Delta z = \frac{F.l^3}{3.E.I_y}$$

$$with: \quad I_y = \frac{w \times t^3}{12}$$

Experimentally, we first made a topographic image of the NS device. Then a force was applied at different points along the beam axis (Fig. 8). We used a specific XYZ feedback loop to ensure very precise XY localization of the AFM tip on the NS beam, the Z loop allowing for very precise control of the applied mechanical force on the NS beam.

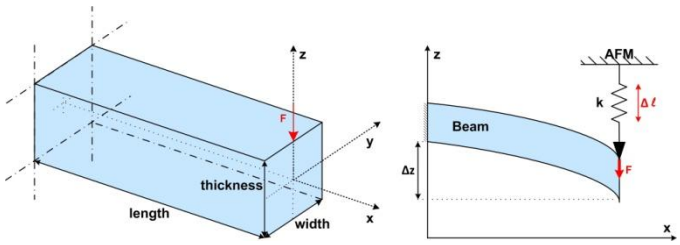

Fig. 7. Schematic of the young modulus extraction model.

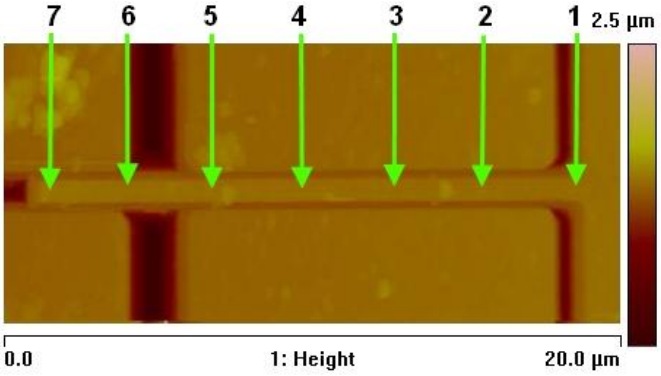

Fig. 8. AFM image of a NS with the position of approach-retract curves.

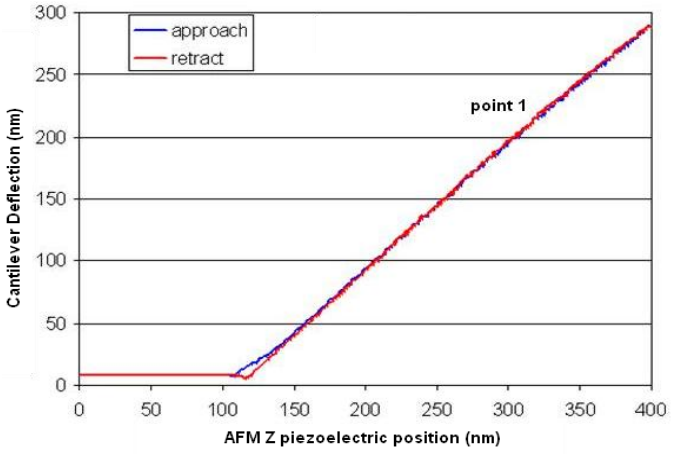

Fig. 9. Approach-retract curve at point 1 (cf. Fig. 8).

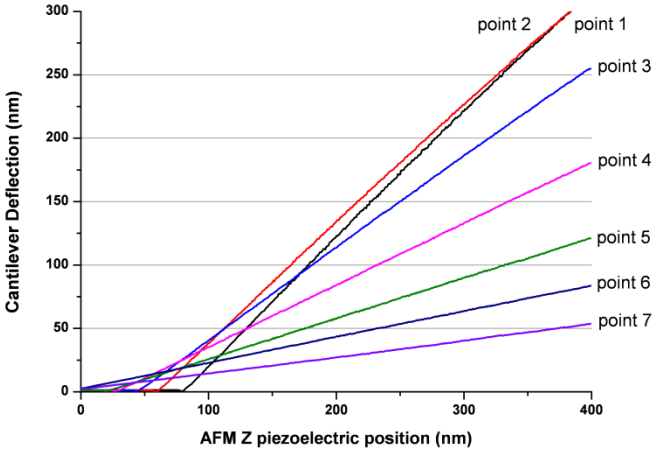

Fig. 10. Approach curves at points 1 to 7 (cf. Fig. 8).

The approach-retract curves (Fig. 9 & 10) show the tip cantilever deflection in function of the AFM Z piezoelectric position. During the approach, the AFM head goes down on the sample. The tip cantilever does not move until it touches the sample. In effect we observe a flat part on curves point 1 to 5 (Fig. 8). The shift and the absence of this flat part on curves point 6 and 7 indicate that the sample was tilted. After touching the sample, the AFM head approach is compensated by the tip cantilever deflection at point 1 and by the beam deflection at point 7. So at point 1 the slop angle of the curve is about 45° because there is no beam to absorb the tip cantilever deflection which is the same that the AFM head position (after had touched the sample). Conversely at point 7 a part of the AFM head movement is compensated by the beam deflection. So the tip cantilever deflection is lower and the slop angle of the curve is lower than at previous points.

From these results, we calculated the force applied by the AFM tip on the beam ($F_{AFM\ TIP}$) and the deflection of beam (Δz_{beam}). We considered that we measured the Young modulus of the bending part of the beam (i. e. from the beam anchor to the AFM probe contact point). Thus in our model, the beam length depends on where we measured the Young modulus along the beam. From the curve $\Delta z_{beam}(F_{AFM\ TIP})$ and using the beam design dimensions (400nm width and 1100 nm thickness), we extracted a beam Young's modulus E of 70 GPa (Fig. 11A). This value is much lower than the mean value from the literature, between 130 and 170 GPa depending on measurement methods, crystal orientation and testing devices (bulk, thin film, beam) [7,8,9].

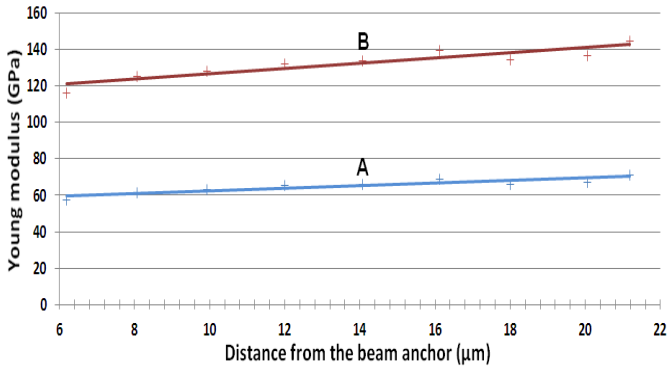

Fig. 11. Extraction of the beam young modulus. A) based on design dimensions. B) based on measured dimensions.

Such a difference can be explained by the polysilicon deposition process [10] but the main reason is the difference on the real dimensions of the beam compared to the design. SEM images showed that the HF etching step to release the beam created an over-etching on the edge of the connection pads (Fig. 3) giving them flexibility. Moreover we extracted the accurate dimensions of beams which are thinner and narrower than expected due to fabrication process (polysilicon deposition and etching). Therefore the beam is more flexible, which explains the lower Vpi and Vpo observed previously. The beam length is an important parameter (see eq. 1) but above all the thickness and the width (Fig. 7) are very critical (affecting Iy) (eq. 1). A beam 110nm thinner than designed (-10%) generates a Young modulus miscalculation higher than 35% (Fig. 12). Finally the side and the edge are not exactly straight, thus changing the beam section shape and also Iy.

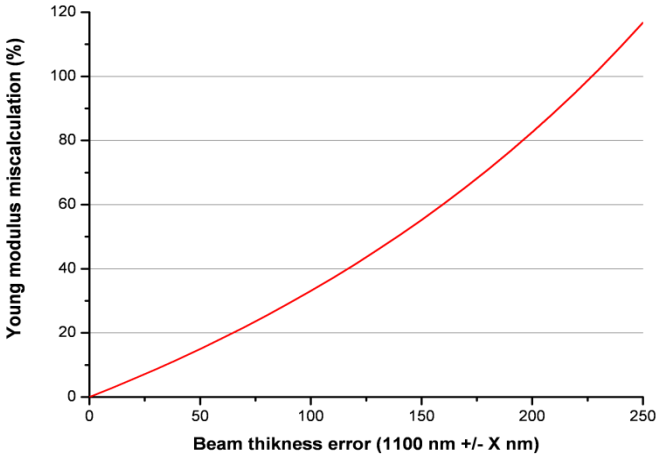

Fig. 12. Young modulus miscalculation depending of the beam thickness error.

Therefore, taking into account the real beam dimensions obtained by SEM and AFM, we found a beam Young's modulus of 140 GPa (Fig. 11B), which is in better agreement with the literature [11,12,13]. We noted the apparent variation of the Young modulus as a function of the distance from the beam anchor, even though the Young modulus is a material property supposed to be constant. This could be due to the influence of the indentation phenomenon and the elastic deformations of the material in our measurement method. To measure the Young modulus of the beam, we measured the absorption of the AFM cantilever deflection by the beam. At the end of the beam, this absorption is mainly due to the beam bending. The indentation phenomenon and the elastic deformations are negligible. On the other end, near the anchor, they are less negligible compared to the beam bending. Thus the total absorption is higher than the absorption due to the beam bending only, so that the beam appears more flexible than in reality, explaining the lower than expected extracted Young modulus. This explains the constant increase of the Young modulus with the distance from the beam anchor. Based on the same principle, we think that the influence of the over-etching is more pronounced near the anchor than at the end of the beam. It makes the beam appear more flexible than expected and therefore underestimation of the Young modulus again. Nevertheless this Young modulus measurement method allowed to improve the beam design and structure with different materials, to study the mechanical reliability of the beam, and is helpful to improve the electromechanical behavior of the NS device.

IV. IMPROVEMENT AND PERSPECTIVES

AFM electrical characterization of the NS beam is important to better understand what happens at the nano-scale during a switching event. To perform in-situ AFM electromechanical characterization [14,15] we have improved the design of the chip, by routing the electrical signals of the different pads (Source, Gate and Drain) to the edge of the chip in order to observe the beam working without disturbing the AFM tip (Fig. 13). In addition, we have also changed the structure of the beam with the deposition of a thin layer of platinum (Fig. 14) on the pads and on all the sidewalls of the

beam to improve the electrical contacts and to solve the problems of oxidation caused by humidity which disturb and stick beams (the metal wall covering is explained in [4,5]). Thanks to platinum the reliability and the yield of NS devices was clearly improved [5].

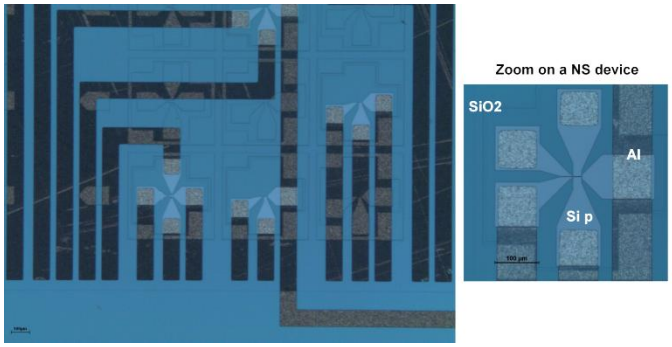

Fig. 13. Optical image of the improved design with electrical contacts routed to the edge of the chip.

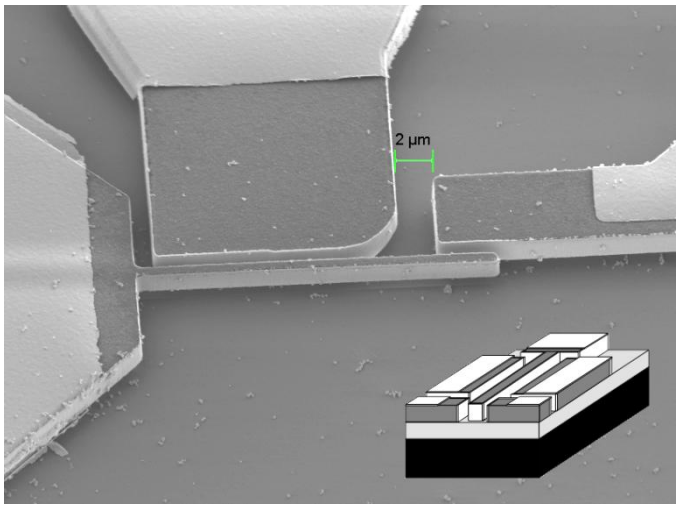

Fig. 14. SEM image showing thin platinum layer coating on the NS side walls to improve the device structure.

V. CONCLUSION

The NS electrical characterization showed a correct behavior, while highlighting a few problems. A deeper analysis using AFM and SEM techniques showed small differences from the designed structure. NS mechanical properties were investigated and the beam Young's modulus was extracted taking account of the real sample characteristics and dimensions which are relevant. NS structure and design was improved. The reliability has been increased and the electrical behavior was better. Finally this innovative technique of characterization will help us to explore new fields of NEMS [16].

ACKNOWLEDGEMENT

Samples were fabricated and designed by Stanford University. They were finalized and customized at the Grenoble Up-line Technological Platform (PTA) which is co-operated by CEA & CNRS within the framework of the French Basic Technology Research (BTR) network. This work has been partly supported by the EU through the Network of Excellence NANOFUNCTION FP7/ICT/NoE (95145). The author would like to thank Xavier Mescot, Martin Gri, Remy Lefevre and Xin Xu for their valuable help.

REFERENCES

[1] K. Akarvardar, et al., "Analytical Modeling of the Suspended-Gate FET and Design Insights for Low-Power Logic," *IEEE Transactions On Electron Devices*, vol. 55, no. 1, p. 48, 2008.

[2] K. Akarvardar, et al., "Design Considerations for Complementary Nanoelectromechanical Logic Gates," *IEDM*, pp. 299-302, 2007.

[3] S. Chong, et al., "Nanoelectromechanical (NEM) Relays Integrated with CMOS SRAM for Improved Stability and Low Leakage," in *ICCAD International Conference on Computer-Aided Design*, 2009.

[4] D. Lee, et al., "Titanium nitride sidewall stringer process for lateral nanoelectromechanical relays," in *MEMS 2010, IEEE 23rd International Conference*, Hong Kong, 2010, pp. 456-459.

[5] R. Parsa, et al., "Composite Polysilicon-Platinum Lateral Nanoelectromechanical Relays," in *14th Solid-State Sensors, Actuators, and Microsystems Workshop*, Hilton Head, South Caroline, 2010, pp. 7-10.

[6] W. C. Young and R. G. Budynas, *Roark's Formulas for Stress and Strain*, 7th ed., McGraw-Hill, Ed. 2002 .

[7] K. R. Virwani, A. P. Malshe, W. F. Schmidt, and D. K. Sood, "Young's modulus measurements of silicon nanostructures using a scanning probe system: a non-destructive evaluation approach," *Smart Materials and Structures*, vol. 12, no. 6, pp. 1028-1032, 2003.

[8] M. A. Hopcroft, W. D. Nix, and T. W. Kenny, "What is the Young's Modulus of Silicon," *Journal Of Microelectromechanical Systems*, vol. 19, no. 2, pp. 229-238, 2010.

[9] C. S. Oh, H. J. Lee, S. G. Ko, S. W. Kim, and H. G. Ahn, "Comparison of the Young's modulus of polysilicon film by tensile testing and nanoindentation," *Sensors and Actuators A*, no. 117, p. 151–158, 2005.

[10] S. Lee, et al., "The effects of post-deposition processes on polysilicon Young's modulus," *Journal of micromechanics and microengineering*, vol. 8, no. 4, pp. 330-337, 1998.

[11] A. San Paulo, J. Bokor, and R. T. Howe, "Mechanical elasticity of single and double clamped silicon nanobeams fabricated by the vapor-liquid-solid method," *Applied Physics Letters*, no. 87, p. 053111, 2005.

[12] J. Wang, Q. A. Huang, and H. Yu, "Young's modulus of silicon nanoplates at finite temperature," *Applied Surface Science*, no. 255, p. 2449–2455, 2008.

[13] C. H. Cho, "Characterization of Young's modulus of silicon versus temperature using a ''beam deflection" method with a four-point bending fixture," *Current Applied Physics*, vol. 9, p. 538–545, 2009.

[14] L. Montès, et al., "AFM Measurement of the Piezoelectric Properties of GaN and GaN/AlN/GaN Individual Nanowires," in *MRS*, San Francisco, 2010.

[15] L. Montès, et al., "Enhancing piezoresistivy and piezoelectricity in nanowire devices," in *IEEE Nano 2010, 12th Nanowire Research Society Meeting*, Seoul, 2010.

[16] X. Xu, et al., "An improved AFM cross-sectional method for piezoelectric nanostructures properties investigation: application to GaN nanowires.," *Nanotechnology*, vol. 22, no. 10, p. 105704, 2011.